Copyright 2018 Society of Photo-Optical Instrumentation Engineers (SPIE). One print or electronic copy may be made for personal use only. Systematic reproduction and distribution, duplication of any material in this paper for a fee or for commercial purposes, or modification of the content of the paper are prohibited.

Hoang Dothe, James W. Duff, Raphael Panfili and Nick Glumac, “NLTERAD (Non-Local Thermodynamic Equilibrium Radiance) Model," Proc. SPIE 10768, Imaging Spectrometry XXII: Applications, Sensors, and Processing, 107680L (18 September 2018).

DOI: https://doi.org/10.1117/12.2321717

See next page for full paper.

Distribution A: Approved for Public Release

NLTERAD (Non-Local Thermodynamic Equilibrium Radiance) Model

H. Dothe*[a], J. W. Duff[a,] R. P. Panfili*[a], Nick Glumac[b]
[a]Spectral Sciences, Inc. 4 Fourth Avenue, Burlington MA 01803-3304;
[b]Mechanical Science and Engineering, University of Illinois Urbana-Champaign, 1206 W. Green Street, Urbana, IL 61801

ABSTRACT

This paper presents an UltraViolet-Visible (UV-Vis) spectral radiance simulation capability for Non-Local Thermodynamic Equilibrium (non-LTE) conditions, consisting of a full line-by-line (LBL) radiative transfer (RT) algorithm and a UV-Vis signatures library. Results are presented for two example scenarios where strong UV-Vis emissions arise, an atmospheric high altitude auroral event and a High Explosive (HE) detonation.

1. INTRODUCTION

Local Thermodynamic Equilibrium (LTE) conditions are achieved by collisional energy transfer between molecules, causing the molecular internal degrees of freedom to reach equilibrium at the local translational temperature. Non-LTE conditions exist when there are not enough molecular excited states formed and lost due to collisions compared to other sources and sinks such as radiative pumping, chemiluminescence, photodissociation and spontaneous emission. These situations occur in, for example, the atmosphere at high altitudes, exhaust plumes and hypersonic wakes. Codes such as NEQAIR[1], SAMM[2,3] and SOCRATES [http://www.spectral.com/our-software/socrates/] model the spectral radiance by explicitly computing the populations of excited states that contribute to the emissions. However in practice, for some of the most extreme non-LTE scenarios, the exact sources of the emissions in the UV-Vis are still unknown, and a spectral radiance simulation capability based on user-input parameters is crucial to model the signatures and identify the emitting species. This paper describes the non-LTE spectral radiance simulation code NLTERAD. In the UV-Vis region, we need to model emissions from highly excited electronic levels arising from extreme non-LTE conditions. For example, solar pumped or electron-impact excitation events, high energy atom molecule, ion molecule collisions in the upper atmosphere, exhaust plumes, missile intercepts, high explosive (HE) detonation, etc., all produce electronic excited states that emit in the UV-Vis region. The desired simulation capability would require as input a simple parameterized description of the states involved the emission along the line-of-sight (LOS). The spatially varying non-LTE conditions along the radiance path also dictates a multi segmented full Radiative Transfer (RT) model, requiring separate parameters for the different segments. Finally, the RT algorithm has to be coupled with a comprehensive spectral library that includes signatures of the possible emitters.

In the following sections, we shall first describe the non-LTE RT formalism and define the key parameters that have to be specified to execute the non-LTE LOS spectral simulation in NLTERAD. We shall next describe the current UV-Vis spectral signatures library that accompanies the code. Finally, two example applications are presented where non-LTE spectra from a high altitude auroral event and a detonation of a High Explosive (HE) are simulated.

Key Words: UV-Vis, Non-LTE, Spectral Signatures, Line-by-line, Forward Model, Radiative Transfer, High Temperature, Simulation

*dothe@spectral.com; phone 781 273-4770; fax 781 270-1161; spectral.com

2. NLTE LINE-BY-LINE RT

For an observer-to-source path of segments *l*, the general expression for the line-of -sight (LOS) spectral emission at frequency ν is given by,

$$I_\nu = \sum_l \left\langle J_\nu^l \right\rangle \left[1 - e^{-\tau_l}\right] e^{-\sum_{m=1}^{l-1} \tau_m} \tag{1}$$

Where τ_l is the optical depth of segment *l* at frequency ν, including contributions from all spectral lines denoted by *i*,

$$\tau_l = \sum_i \tau_{li} = \sum_i \kappa_{\nu i}^l \, \rho_i''(l) L_l \tag{2}$$

In Eq. (2), ρ_i'' is the density of lower state in spectral line *i*, and L_l is the segment length. The $\kappa_{\nu i}^l$ are absorption coefficients in segment *l* by spectral line *i*.

The key frequency dependent quantities in Eq. (1) are thus the emission source and the absorption coefficients. The general non-LTE expressions for both emission source and absorption terms are now described in the next two sections.

2.1 Non-LTE emission source

For a single transition line $i = \eta' \rightarrow \eta$ where η and η' denote the lower and upper states, respectively, the non-LTE source term at frequency ν is defined as,

$$J_\nu = \frac{c_1 \nu^3}{\pi} \left[\frac{Z_{\eta'\eta}}{1 - Z_{\eta'\eta}} \right] \tag{3}$$

Where we have defined the population ratio of upper state η' to lower state η as, $Z_{\eta'\eta} = \dfrac{N_{\eta'}/d_{\eta'}}{N_\eta/d_\eta}$.

N and *d* denote the population and degeneracy of the states. We note that N_η is the same as ρ_i'' in Eq. (2)

The averaged source terms at frequency ν for segment *l* in Eq. (1), $\left\langle J_\nu^l \right\rangle$, include contributions from all spectral lines *i*, each weighted by the corresponding optical depth τ_{li}.

2.2 Non-LTE absorption coefficient

The absorption coefficient at frequency ν due spectral line *i* is given by,

$$\kappa_{\nu i} = S_i f_{\nu i} \tag{4}$$

Where S_i is the line strength for the transition line *i* from η to η' and $f_{\nu i}$ is the value of the pressure and temperature dependent spectral line shape function at ν.

S_i can be defined for either LTE or non-LTE conditions. To model emissions from highly excited electronic levels arising from extreme non-LTE conditions, a non-LTE expression for the line strength, $S_i = S_{\eta\eta'}^{NLTE}$, is required. It is based on an extension of the general expression for the LTE line strength[4] given at a reference temperature T_{ref}.

$$S_{\eta\eta'}^{LTE} = \frac{8\pi^3}{3hc} I_a \frac{d_\eta e^{-c_2 E_\eta / T_{ref}}}{Q} \nu \left[1 - e^{-c_2 \nu / T_{ref}}\right] \frac{1}{d_\eta} \left|R_{\eta\eta'}\right|^2 \quad \textbf{(5)}$$

Where I_a is the abundance factor for the species, E_η is the lower state energy, ν is the energy spacing (both in cm-1), c_2 is the second radiation constant, Q is the total partition function at T_{ref}, and $\left|R_{\eta\eta'}\right|^2$ is the transition dipole moment squared.

The non-LTE line strength is computed from the LTE expression by using the non-LTE population ratios,

$$S_{\eta\eta'}^{NLTE} = N_\eta \left[1 - Z_{\eta'\eta}\right] S_{\eta\eta'}^0 \quad \textbf{(6)}$$

Where $S_{\eta\eta'}^0$ is the temperature dependent expression derived from Eq. (5)

$$\begin{aligned} S_{\eta\eta'}^0 &= S_{\eta\eta'}^{LTE} Q\, e^{c_2 E_\eta / T_{ref}} \left[1 - e^{-c_2 \nu / T_{ref}}\right]^{-1} \\ &= \frac{8\pi^3}{3hc} I_a \nu \frac{1}{d_\eta} \left|R_{\eta\eta'}\right|^2 \end{aligned} \quad \textbf{(7)}$$

Eqs (3), (4) and (6) show that the key quantities describing non-LTE conditions in both emission source and absorption terms are the population ratios $Z_{\eta'\eta}$.

In the non-LTE radiance models SHARC[5]/SAMM[2,3] the populations of the excited states η and η' are directly computed by solving a set of chemical kinetic equations describing the production and loss mechanisms for those states. The population ratios $Z_{\eta'\eta}$ are then obtained, and the spectral radiance calculated via Eq. (1). For the spectral simulation model, it is useful to define a convenient input parameter to parameterize these ratios.

The concept of vibrational/vibronic temperatures is now introduced as the most convenient parameters and thus the most logical inputs for our spectral simulation model.

2.3 Vibrational and vibronic temperatures

A temperature parameter is usually introduced to describe the population ratio,

$$T_{NLTE} = -c_2 \nu / \ln Z_{\eta'\eta} \quad \textbf{(8)}$$

where T_{NLTE} has units of *K*, ν is the energy spacing (in cm^{-1}) and c_2 is the second radiation constant. The expression for the non-LTE emission source and line strength can then be rewritten in terms of T_{NLTE} as,

$$J_\nu = \frac{c_1 \nu^3}{\pi} \left[\frac{e^{-c_2 \nu / T_{NLTE}}}{1 - e^{-c_2 \nu / T_{NLTE}}}\right] = \frac{c_1 \nu^3}{\pi} \left[\frac{1}{e^{c_2 \nu / T_{NLTE}} - 1}\right] \quad \textbf{(9)}$$

and

$$S_{\eta\eta'}^{NLTE} = N_\eta \left[1 - e^{-c_2 \nu / T_{NLTE}}\right] S_{\eta\eta'}^0 \quad \textbf{(10)}$$

It should be pointed out that the concept of temperature introduced here does not necessarily imply any equilibrium condition among any of the molecular internal degree of freedoms, but is simply a convenient parameter to describe the key quantity that describes the non-LTE radiance, i.e., the population ratio.

However, there are various degrees of non-LTE conditions that do allow us to make further approximations to T_{NLTE}. For example, expressing the energy spacings in terms of their separate electronic, vibrational and rotational contributions $\left(\nu = \nu_{el} + \nu_{vib} + \nu_{rot}\right)$, we can assume the separate internal motions to be described by separate temperatures. Using Boltzman factors at the separate temperatures to express the population ratios, Eq. (9) can be rewritten as,

$$J_\nu = \frac{c_1 \nu^3}{\pi}\left[\frac{1}{e^{c_2\left(\nu_{el}/T_{el} + \nu_{vib}/T_{vib} + \nu_{rot}/T_{rot}\right)} - 1}\right] \tag{11}$$

Similarly, taking into account the separate degrees of freedom for the partition functions, Eq. (10) can be rewritten for the full non-LTE conditions $\left(T_{el} \neq T_{vib} \neq T_{rot}\right)$ as,

$$S_{\eta\eta'}^{NLTE} = \frac{e^{-c_2 E_{el}^{\eta}/T_{el}}}{Q_{el}} \cdot \frac{e^{-c_2 E_{vib}^{\eta}/T_{vib}}}{Q_{vib}} \cdot \frac{e^{-c_2 E_{rot}^{\eta}/T_{rot}}}{Q_{rot}} \times \left[1 - e^{-c_2\left(\nu_{el}/T_{el} + \nu_{vib}/T_{vib} + \nu_{rot}/T_{rot}\right)}\right] S_{\eta\eta'}^{0} \tag{12}$$

In practical applications, there are situations where some molecular degree of freedom i.e., electronic/vibrational, may be in non-LTE while others remain in equilibrium, e.g., rotational. We describe below two spectral regions where those situations apply.

2.3.1 IR spectral region: vibrational/rotational temperatures

In the IR spectral region where signatures arise from transitions between vibrational levels within the same electronic level, the electronic degree of freedom can essentially be ignored. Thus only two temperature parameters need to be specified in Eq. (11) and (12) for the IR, T_{vib} and T_{rot}, together with the kinetic temperature T_{kin}. In the atmosphere, T_{rot} is also often set equal to T_{kin} in each LOS segment, assuming that the rotational motion reaches equilibrium the fastest. This is indeed the assumption taken in the non-LTE radiance code SHARC[5] and SAMM[2,3].

2.3.2 UV-Vis spectral region: vibronic temperature approximation

The approach taken for IR applications can be extended into the UV-Vis.

Spectral signature simulation models can be used to identify and analyze the UV-Vis molecular bands in observed data that arise from transitions between electronic-vibrational levels, or vibronic levels of emitting species. The line positions are determined by the electronic-vibrational energy differences between the upper and lower states. It is therefore common to combine the electronic and vibrational energies of a given state into the vibronic energy, $E_{vibron} = E_{el} + E_{vib}$, then T_{vibron} can be used as a parameter to specify transitions in the UV-Vis in the same way that T_{vib} is used for the IR. Only two temperature parameters need thus be specified in Eq. (9a) and (10a) for the UV-Vis, T_{vibron} and T_{rot}, together with the kinetic temperature T_{kin}.

It should be noted that while it may be more rigorous to further separate the vibronic energy into separate electronic and vibrational components and use Eqs (11) and (12) in their full form, there is usually not sufficient information to specify the distinct temperatures T_{el} and T_{vib} . It is sufficient and more straightforward to use T_{vibron} as a parameter in our spectral simulation model.

3. UV-VIS SPECTRAL LIBRARY

The UV-Vis spectral library include signatures for diatomic neutral and ionic molecules that appear in non-LTE conditions in high altitude atmosphere, high energy atom molecule, ion molecule collisions in exhaust plumes, missile intercept plasmas, high explosive (HE) detonation. The current list include most of the diatomic species formed by C, N, H and O, as well as N_2^+, and is still being updated. The transition line data for most diatomics are taken from Kurucz[7].

For the N_2 and N_2^+ transitions, the line data from the Atmospheric Ultraviolet Radiance Integrated Code (AURIC)[6] were adopted.

Examples are shown below for the CO(A-X), CO(a-X), N_2(a-X), N_2(B-A) and N_2(C-B) at high vibronic and rotational temperatures. Examples for these transitions are illustrated in Figures 1, 2, 3, 4 and 5 respectively. Intensities are shown for a column density of 1.5×10^{12} molecules/cm^2, and vibronic and rotational temperatures of 5000K and 1000K, respectively.

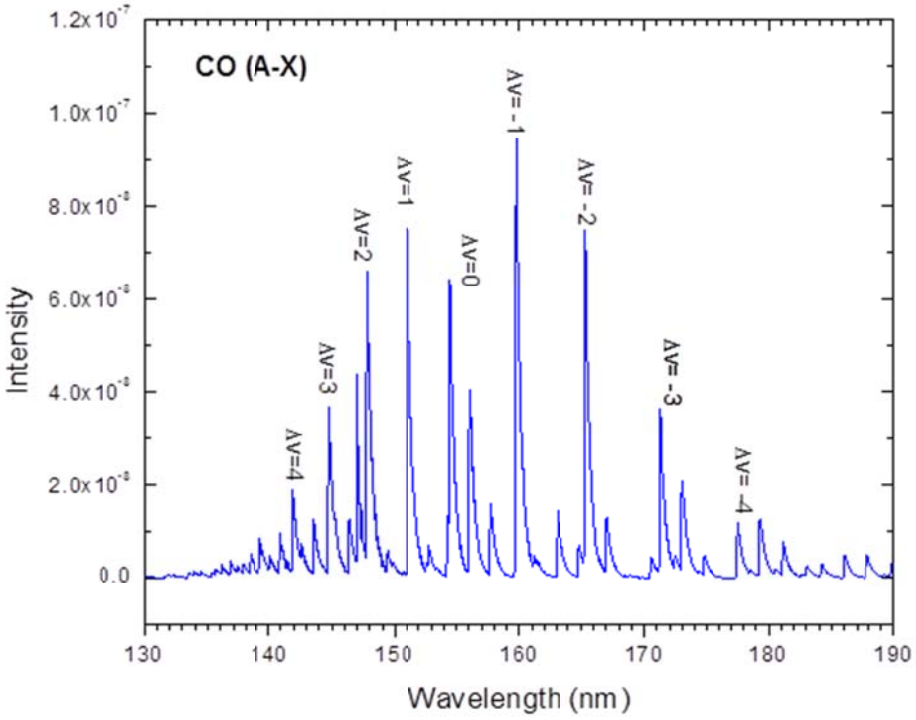

Figure 1. Intensity of the CO (A-X) electronic transition (Fourth Positive band). Intensity in W/cm^2/sr/nm.

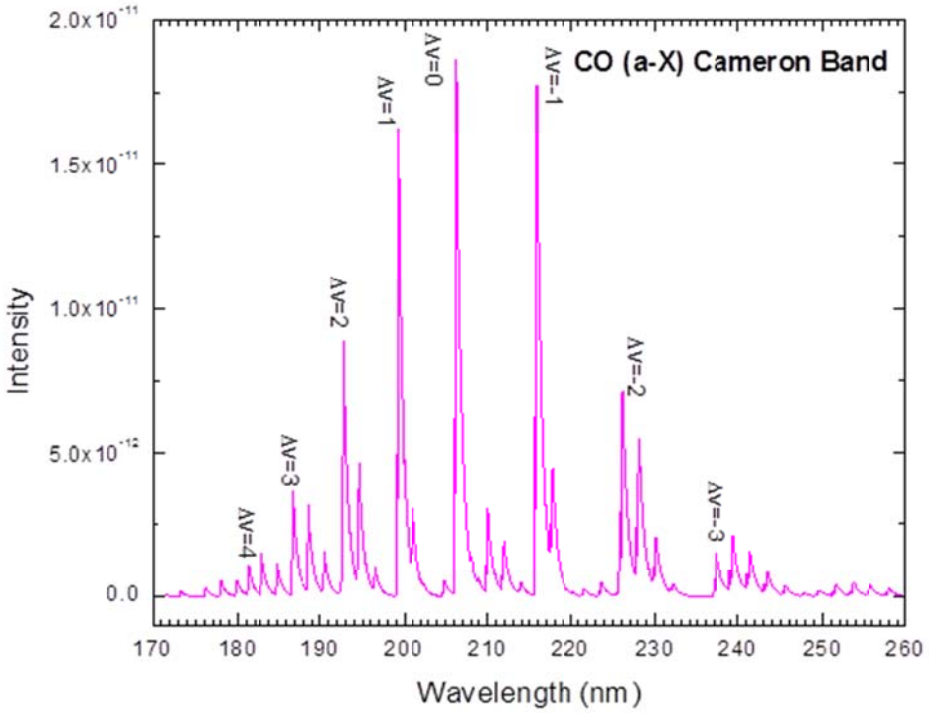

Figure 2. Intensity of the CO (a-X) electronic transition (Cameron band). Intensity in W/cm^2/sr/nm.

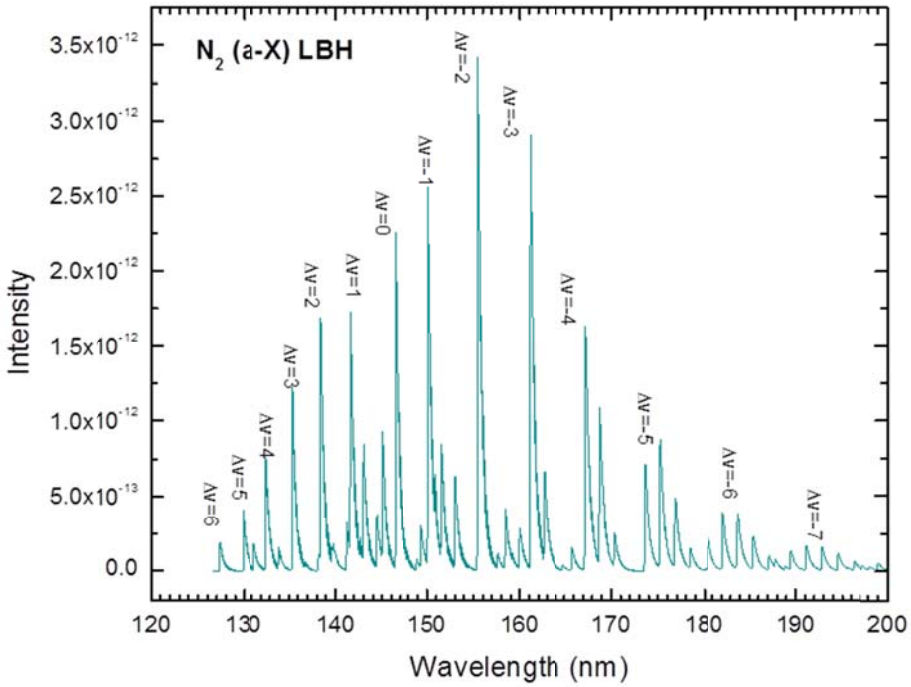

Figure 3. Intensity of the N_2(a-X) electronic transition (LBH band). Intensity in W/cm^2/sr/nm.

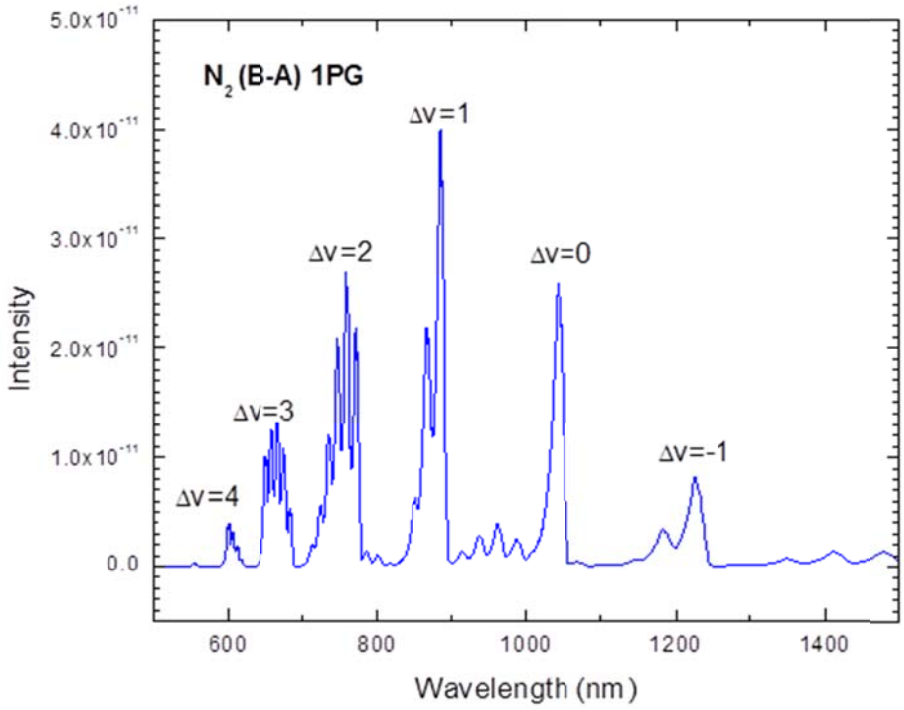

Figure 4. Intensity of the N_2 (B-A) electronic transition (1st Positive). Intensity in W/cm^2/sr/nm.

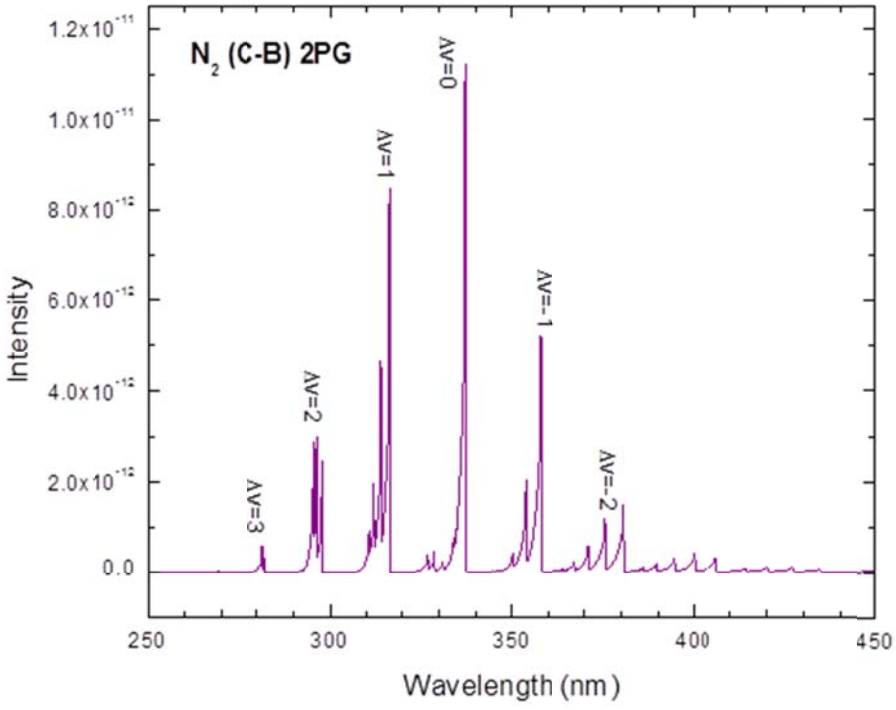

Figure 5. Intensity of the N_2 (C-B) electronic transition (2nd Positive). Intensity in W/cm^2/sr/nm.

4. EXAMPLES

We now present some example applications of the NLTERAD spectral radiance simulation code.

4.1 Auroral N_2^+ radiance:SAMM vs NLTERAD

Figure 6 illustrates the N_2^+ limb emission spectrum computed for an auroral event by SAMM at a tangent height of ~ 100km. The SAMM spectrum is computed from Eq. (1) using excited state populations obtained by directly solving the kinetic equations for the sources and sinks of N_2^+ under auroral conditions. SAMM calculations of this type have been previously used to successfully model the N_2^+ auroral radiance observed by the MSX satellite[8]. For the results shown in Figure 6, we used a Maxwellian electron energy distribution with total energy flux of 100ergs/cm^2/sec and characteristic energy of 5keV. The aurorally dosed region was between the latitudes [60^o,70 ^{o}] and longitudes [-10 ^{o}.10 ^{o}] and the aurora duration was 100 sec.

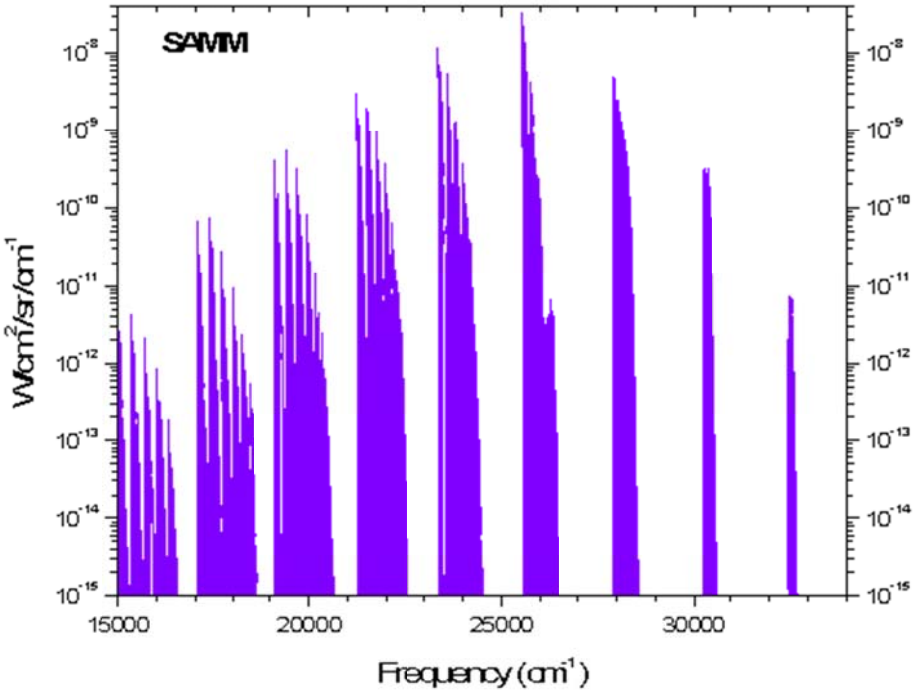

Figure 6. N_2^+ limb emission spectrum computed for an auroral event by SAMM at a tangent height of ~ 100km. The raw SAMM spectra have been degraded with a triangular function of 1 cm^{-1} half width.

At these high altitudes, the LOS emission is optically thin, so a spectral radiance simulation can be performed by using as parameters an effective N_2^+ column density and a set vibronic/rotational temperatures for a single LOS segment NLTERAD run. Figure 7 illustrates the NLTERAD results with a column density of 4x10^{12} molec/cm^2, vibronic temperature of 2500K and rotational temperature of 300K.

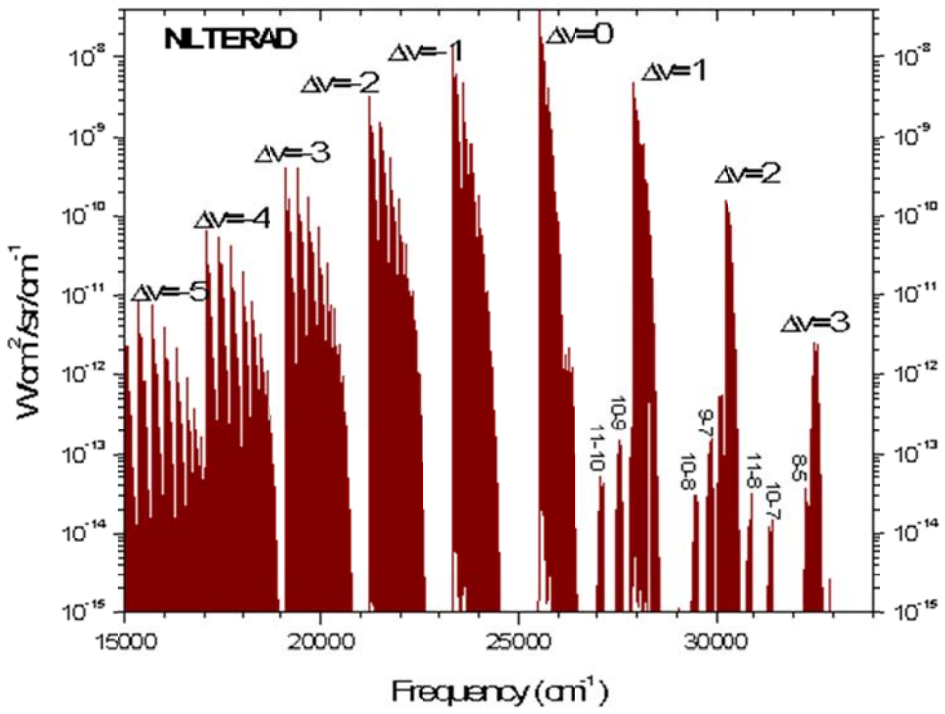

Figure 7. NLTERAD simulation with a column density of $4x10^{12}$ molec/cm^2, vibronic temperature of 2500K and rotational temperature of 300K. The raw non-LTE spectra have been degraded with a triangular function of 1 cm-1 half width.

In Figures 6 and 7, the SAMM and NLTERAD spectral radiances have been plotted on a logarithmic scale to make detailed comparisons possible. It can be seen that while the two spectra are in good agreement for all of the manifolds (Δv=-5, -4, -3, -2, -1, 0, 1, 2, 3), the NLTERAD spectrum shows more bands (v'→v) than the SAMM results. This is due to the fact that the N_2^+ signature database has been upgraded for NLTERAD, including transitions between vibrational states up to v=11 for both upper and lower electronic levels of the N_2^+ B-X band, while the SAMM library does not include vibrational states greater than 5. Nevertheless, the general good agreement shows the NLTERAD capability of simulating an auroral UV-Vis spectrum using suitable parameters for column densities and vibronic/rotational temperatures.

The above example also indicates the practical usefulness of the NLTERAD approach of identifying and analyzing spectral signatures when the user is presented with an optically thin spectrum such as Figure 6. The next example illustrates a more challenging application where opacity effects occur along the radiance path.

4.2 HE detonation spectra

The detonation of HE produces many atomic and diatomic species and enough energy is released early in the detonation time line to create many electronic states, giving rise to various UV-Vis emissions that can be experimentally observed[9]. The energy release in detonation is analogous to that occurring in missile intercept events which have been previously investigated, both events producing early plasma conditions where atomic emissions dominate, and later molecular emissions from species formed in interactions with the atmosphere[10-11]. Examples of detonation spectra as functions of time are shown in Figure 8a and 8b for the detonation of PETN in Air, for the time periods 0μs-2μs and 4μs -10μs, respectively[12]. It is seen that at the very early times (0μs -2μs), the spectral data show emission features from various species above a background continuum, while at later times (4μs -10μs), more opaque conditions occur where the emission features recede and absorption features appear.

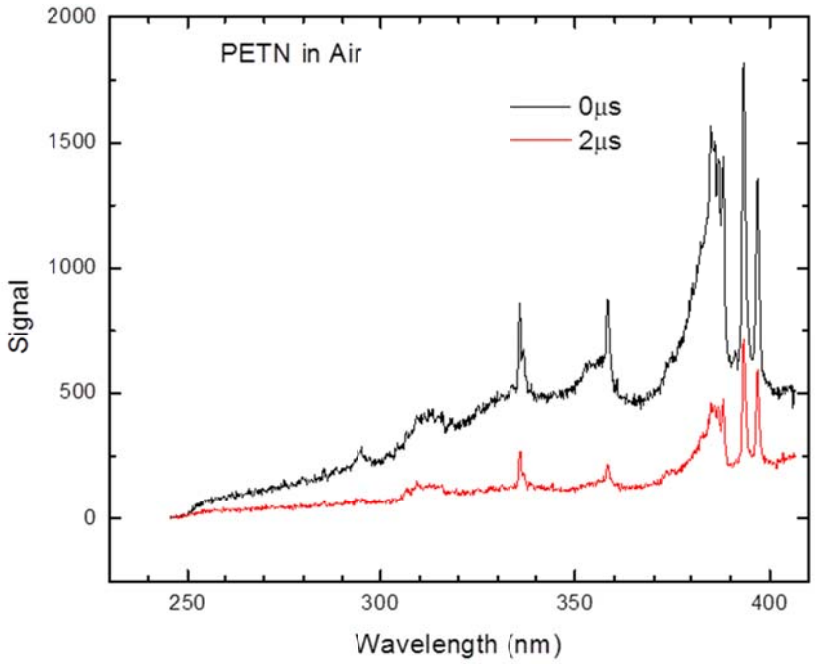

Figure 8a. Observed spectra of the detonation of PETN in Air at early times 0μs -2μs.

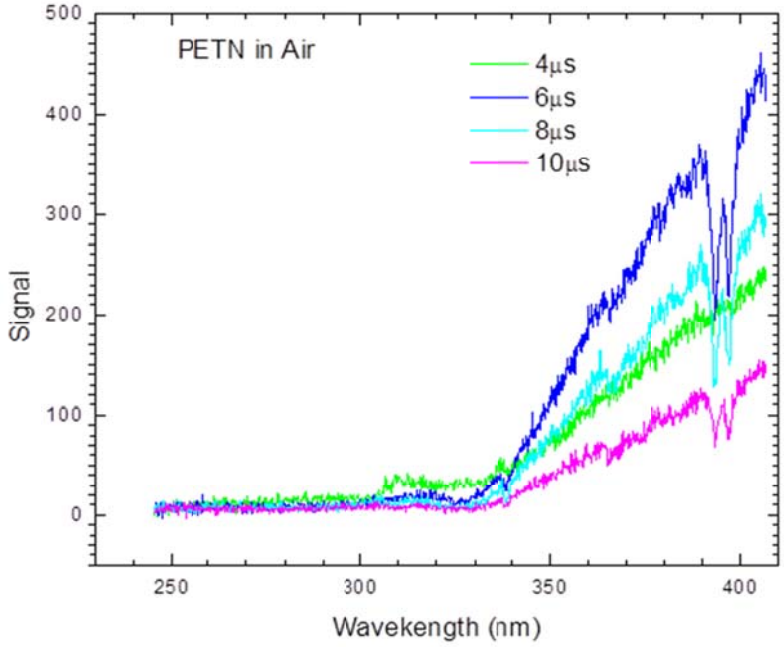

Figure 8b. Observed spectra of the detonation of PETN in Air at later times 4μs -10μs.

This situation is unlike the optically thin situation in the auroral event illustrated above when a single layer RT model is sufficient. Modeling this situation where non LTE effects exist along the radiance path requires a multi segmented RT capability such as NLTERAD. While simulation codes such as LIFBASE[13] [http://www.sri.com/cem/lifbase] and Specair [http://www.specair-radiation.net/] have the spectral library to reproduce the observed signatures, they do not have the built in RT to describe the varying non LTE effects along the path as exhibited in Figures 8a and 8b. (It should however be noted that Specair does allow for the effect of absorption by room air between the emitting gas or plasma and the detector, i.e., by H_2O and CO_2 in the infrared and O_2 Schuman-Runge continuum below 185 nm).

In our NLTERAD simulation of the detonation of PETN in Air, we have used a two segment model where the inner segment (farthest to the observer) is described by a gray body function representing the observed background continuum, and the outer segment (closest to the observer) contains the various emitting/absorbing atomic and molecular species.

It should be pointed out that the signal data in Figure 8a and 8b are not in absolute intensity units so only relative intensities of emission/absorption contributions from the various species can be used to evaluate the NLTERAD simulation results. Therefore, we have assumed a black body function for the continuum background and our simulation parameters are, 1) in the inner segment, the black body temperature and 2) in the outer segment, for each possible species with signatures in the spectral band pass, a column density and a set of vibronic/rotational temperatures for each separate transition band.

Figures 9a and 9b show the NLTERAD results. We have chosen to show spectra that simulate the emission features at time t=0μs, and the emission/absorption features at t=6μs, to represent the NLTERAD capability to model both the early and later times observations.

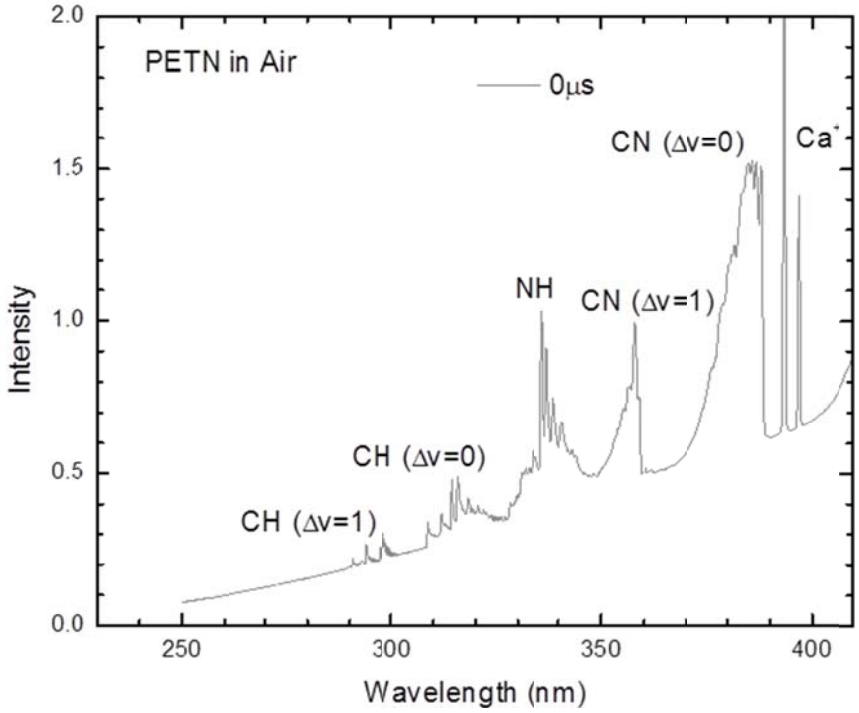

Figure 9a. NLTERAD simulated spectra of the detonation of PETN in Air at t= 0μs.

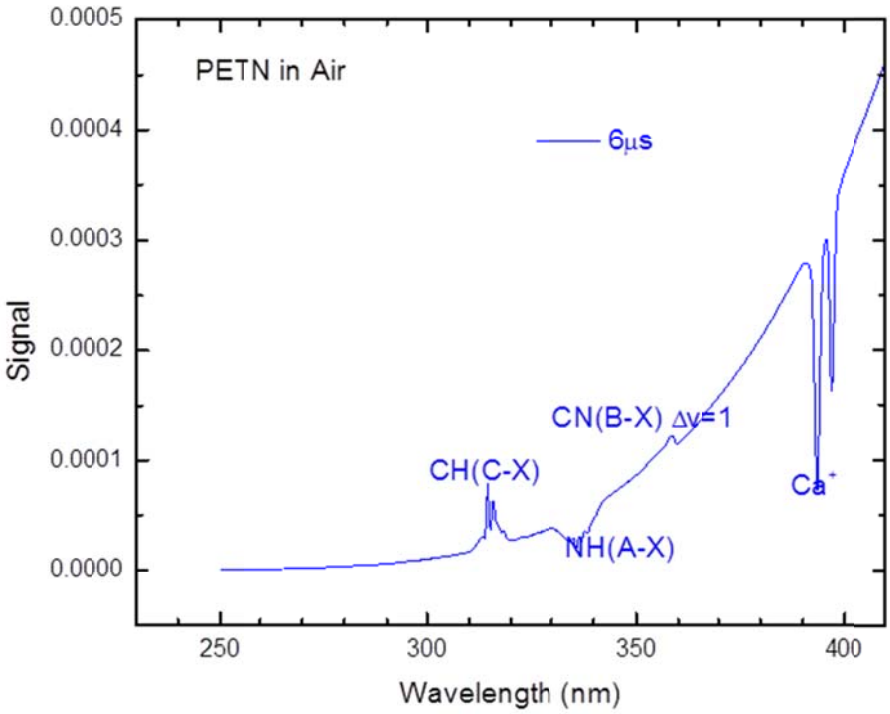

Figure 9b. NLTERAD simulated spectra of the detonation of PETN in Air at t= 6μs.

At the time this paper is prepared, it is found that both OH (A-X) and CH (C-X) are candidates to model the observed features near 310 nm. While results for CH (C-X) are shown in Figs 9A and 9B to illustrate the NLTERAD capability, a definite identification awaits the availability of higher resolution data and is beyond the scope of the current paper.

For our two segment non-LTE model, the black body temperature of the inner segment plays an important role in determining whether emission or absorption features occur in the LOS radiance. If the vibronic or electronic temperature of a given band for a particular molecular or atomic species in the outer segment is greater (less) than the black body temperature of the inner segment, emission (absorption) features will result from that band in the total spectral radiance.

In Figure 9A for t=0μs, the vibronic/rotational temperatures are 5500K/4000K, 5200K/5000K, 5400K/5000K, 5500K/5000K for CH(C-X, Δv =0 and Δv =1), NH(A-X, Δv =0), CN(B-X, Δv =1) and CN(B-X, Δv =0), respectively, and the electronic temperature for Ca+ is 8000K. All the vibronic/electronic temperatures for all the species are thus greater than the blackbody temperature which is 4800K, resulting in the emission features above the continuum background, as observed in Figure 8A.

In Figure 9B for t=6μs, the vibronic/rotational temperatures are 2800K/1000K, 2200K/1000K, 2800K/10000K for CH(C-X, Δv =0) , NH(A-X, Δv =0) and CN(B-X, Δv =1), respectively, and the electronic temperature for Ca^+ is 1500K. The black body temperature is 2400K, thus we have emission features from CH(A-X, Δv =0) and CN(B-X, Δv =1), and absorption features from NH(A-X, (Δv =0) and Ca^+, as observed in Figure 8B.

It should be pointed out that for any molecular species, NLTERAD allows each Dv manifold in each electronic transition to be described by a separate set of vibronic/rotational temperature. This capability was used in modeling the Δv =0 and Δv =1 manifolds of the CN (B-X) band. In Fig. 9A for t=0μs, the vibronic temperatures for the Δv =0 and Δv =1 manifolds are 5500K and 5400K, respectively while the rotational temperature is 5000K for both. In Fig. 9B for t=6μs, the vibronic temperature for the Δv =1 manifold is 2800K while that for the Δv =0 manifold equal to the black body temperature at 2400K.

5. CONCLUSIONS

The practicality of the NLTERAD approach of identifying and analyzing spectral signatures has been demonstrated by applications in both optical thin and opaque scenarios. The multi-segment non-LTE RT capability was able to simulate the varying non-LTE effects along the radiance path exhibited by the emission and absorption features observed in the time series of detonation spectra of PETN in Air. The good agreement between the SAMM computed auroral spectra and NLTERAD simulated spectra points to the possibility of interfacing the NLTERAD RT module with vibronic temperatures derived from separate existing and future kinetic modules designed for diverse non-LTE phenomena to predict non-LTE spectral radiance.

6. ACKNOWLEDGEMENT

We would like to express our thanks to the Missile Defense Agency (MDA) for having supported the development of all the underlying technologies over the years that have contributed to the development of the non-LTE radiance algorithm presented in this work. This work was also made possible by an Air Force SBIR award to analyze HE detonation spectra and we would like to thank Dr. Stephanie Johnson for her support and guidance.

7. REFERENCES

[1] Whiting, E., L. Yen, J. Arnold, and J. Patterson, "NEQAIR96, Nonequilibrium and Equilibrium Radiative Transport and Spectra Program: Users' Manual," Technical Report No. NASA RP-1389, (1996).

[2] Dothe, H., J.W. Duff, J.H. Gruninger, P.K. Acharya, A. Berk, and J. H. Brown, "Users' manual for SAMM®2, SHARC-4 and MODTRAN®4 merged," AFRL-VS-HA-TR-2004-1001 (2004).

[3] Panfili, R., H. Dothe, J.H. Gruninger, J.W. Duff, and J.H. Brown, "All-Altitude Atmospheric Radiation Transport with SAMM2," AIP Conference Proceedings 1100, 77 (2009).

[4] Gamache, R. R. and L. S. Rothman, "Extension of the HITRAN Database to non-LTE Applications", J. Quant.Spectrosc. Radiat. Transfer, Vol. 48, No. 5/6, pp 519-525, (1992)

[5] Sundberg, R. L. et al., "SHARC, a model for calculating atmospheric infrared radiation under non-equilibrium conditions", Geophys. Monogr. Ser., vol. 87, edited by R. M. Johnson and T. L. Killeen, pp. 287-295, AGU, Washington, D. C., (1995)

[6] Strickland, D.J., J. Bishop, J.S. Evans, T. Majeed, P.M. Shen, R.J. Cox, R. Link, and R.E. Huffman, Atmospheric Ultraviolet Radiance Integrated Code (AURIC): theory, software architecture, inputs, and selected results, Journal of Quantitative Spectroscopy & Radiative Transfer, 62(6), 689-742, doi:10.1016/S0022-4073(98)00098-3, (1999).

[7] Kurucz, R. L., "Molecular Database: http://kurucz.harvard.edu/molecules.html," Smithsonian Astrophysical Observatory, Cambridge, MA, (2015).

[8] Dothe, H., J. W. Duff, J. H. Gruninger, R. Panfili, R. Kennett and J. H. Brown, "Auroral Radiance Modeling with SAMM®2," Proceedings of SPIE, 7475, 747509, (2009).

[9] Glumac, N., "Early time spectroscopic measurements during high-explosive detonation breakout into air," Shock Waves (2013) 23:131138.

[10] Bernstein, L.S., J. W. Duff, A. Hosangadi, S. Dash, G. Wren, and W. Oberle, "Analysis of plasma radiation effects in electrothermal chemical gun propulsion," Proceedings of the JANNAF Combustion Symposium, (1998).

[11] Bernstein, L.S., Braunstein, M., Allen, J., Gibson, D. and Kiessling, J., "Analyses of the IR Signature from a High-Altitude Intercept Debris Cloud," 11th Annual AIAA/MDA Technology Conference and Exhibit, Monterey, CA, (2002).

[12] Glumac, N., Private Communications, (2016).

[13] Luque, J. and D. R. Crosley, J. Luque and D.R. Crosley, "LIFBASE: Database and Spectral Simulation Program (Version 1.5) ", SRI International Report MP 99-009 (1999).